Measurement 234 (2024) 114885

Contents lists available at ScienceDirect

Measurement

journal homepage: www.elsevier.com/locate/measurement

Generalized multi-point interpolated DTFT frequency and damping factor estimators of real-valued damped sinusoids

Daniel Belega [a,*], Dario Petri [b], Dominique Dallet [c]

[a] Department of Measurements and Optical Electronics, Politehnica University Timişoara, Bv. V. Pârvan, Nr. 2, 300223 Timişoara, Romania
[b] Department of Industrial Engineering, University of Trento, Trento 38123, Italy
[c] IMS Laboratory, Bordeaux INP, University of Bordeaux, CNRS UMR5218, 351 Cours de la Libération, Bâtiment A31, 33405 Talence Cedex, France

ARTICLE INFO

Keywords:
Interpolated discrete-time Fourier transform
Parameter estimation
Real-valued damped sinusoid
Signal windowing

ABSTRACT

In this paper a generalized multi-point interpolated Discrete-Time Fourier Transform (DTFT) is proposed for frequency and damping factor estimation of real-valued damped sinusoids. The acquired data are weighted by a Maximum Sidelobe Decay (MSD) window and the interpolation function is defined as the ratio between two linear combinations of DTFT samples located one bin apart, which is generalized exploiting a tuning parameter. Analytical expressions for the estimated parameter errors due to the interference of the fundamental image component are derived. Leveraging on these expressions an improved version of the algorithm is also proposed and optimized by selecting a suitable value for the tuning parameter. The developed theory is applied to both a three-point and a four-point interpolated Discrete Fourier Transform (IpDFT) estimators published in the literature and the achieved accuracy improvements are verified through simulations.

1. Introduction

Damped sinusoids have a crucial role in many application areas such as radar, nuclear magnetic resonance, optics, and mechanics [1–5]. The unknown signal parameters can be estimated through either parametric or non-parametric algorithms. The parametric algorithms such as the Prony algorithm, the Steiglitz-McBride algorithm (iterative Prony algorithm), and the Matrix Pencil algorithm [4,6,7] provide accurate parameter estimates, but require a high processing effort since they imply computationally expensive matrix operations. Conversely, non-parametric algorithms operate in the frequency-domain and may return accurate parameters estimates with low computational effort. Thus, they are usually preferred in real-time applications. Among these algorithms, the so-called Interpolated Discrete-Time Fourier Transform (IpDTFT) algorithms are often employed due to their relative simplicity [3,5,8–18]. According to these algorithms, accurate frequency and damping factor estimates are obtained by interpolating two or more relevant Discrete-Time Fourier Transform (DTFT) samples of the analyzed signal, so compensating the picket-fence effect due to the finite number of analyzed samples [3,5,8–18]. However, when only a few cycles of real-valued damped sinusoids are processed, the effect of the fundamental image component on estimation accuracy can be significant. To reduce that contribution two approaches have been proposed in the literature. The first one consists in interpolating more than two DTFT samples [3,11,12], while the second one is based on the compensation of the image component contribution [13–18]. In [3] the accuracies of the frequency and the damping factor estimates returned by some three-point and four-point IpDFT (3p-IpDFT and 4p-IpDFT) algorithms have been analyzed. In [11] a 3p-IpDFT algorithm proposed for the parameter estimation of real-valued undamped sinusoid [21] has been extended to damped sinusoids and a damping factor estimator has been derived when either the rectangular or the Hann windows are applied. The accuracy of the multi-point IpDFT algorithms has been investigated in both [3] and [11] through computer simulations, but the case when only a few signal cycles are available has not be considered. In [13–18] two-point IpDFT (2p-IpDFT) and 3p-IpDFT algorithms have been proposed to compensate the detrimental effect of the fundamental image component on the estimated parameters. The algorithms proposed in [13] and [14] consider a rectangular windowing and several analytical expressions must be evaluated to obtain an estimation of the unknown parameters. In addition, the zero-padding is used in [14] to achieve accuracies higher than those of the algorithm proposed in [13]. Conversely, in [15] the algorithm proposed in [5] for rectangular window is extended to the Maximum Sidelobe Decay (MSD)

* Corresponding author.
E-mail addresses: daniel.belega@upt.ro (D. Belega), dario.petri@unitn.it (D. Petri), dominique.dallet@ims-bordeaux.fr (D. Dallet).

https://doi.org/10.1016/j.measurement.2024.114885
Received 14 February 2024; Received in revised form 1 May 2024; Accepted 8 May 2024
Available online 10 May 2024

windows [19] and then the contribution of the fundamental image component on the estimated parameters is compensated. It is worth noticing that the MSD windows allow a great reduction of the effect on the estimated parameters of the possible interfering spectral tones due to their high spectral leakage suppression capability [20]. The 3p-IpDFT algorithms proposed in [16] and [17] are based on the rectangular window and the compensation of the fundamental image component contribution is quite computationally expensive. In [17] also a more accurate version of the algorithm obtained through zero-padding is proposed. However, neither [16] nor [17] analyze the effect of possible spurious tones on parameter estimation accuracy. In [18] a well-known complex-valued undamped sinusoid 3p-IpDFT frequency estimator [22–24] has been extended to real-valued damped sinusoids weighted by a generic MSD window and analytically simple estimators have been derived. Moreover, the analysis of the impact of the fundamental image component on the estimated parameters enabled the derivation of a new computationally inexpensive 3p-IpDFT algorithm capable to provide more accurate estimates than the published one when only short observations are available.

In this paper a generalized multi-point IpDTFT frequency and damping factor estimator of real-valued damped sinusoid is proposed. The acquired data are weighted by an MSD window and the interpolation function is defined as the ratio between two linear combinations of DTFT samples located one bin apart, which is generalized through a tuning parameter. Analytical expressions for the estimated parameter errors due to the interference from the fundamental image component are derived. Leveraging on the derived expressions a more accurate version of the algorithm is then proposed and optimized by a suitable choice of the tuning parameter value. The obtained results are applied to already published 3p-IpDFT and 4p-IpDFT algorithms so improving their estimation accuracy. Thus, the main contributions of this work are as follows:

- proposal of an approach that allows to increase the accuracy of any multi-point IpDFT algorithm based on an interpolation function defined as the ratio between two linear combinations of DTFT samples located one bin apart;
- signal weighting by MSD windows so ensuring a high rejection of the contribution of possible spurious tones on the estimated parameters.

The remaining part of this paper is organized as follows. In Section 2 the generalized multi-point interpolation function is presented. Expressions for the related frequency and damping factor estimation errors due to the interference from the fundamental image component are derived and an algorithm that compensates these detrimental contributions is proposed and optimized. In Section 3 the developed theory is applied to the 3p-IpDFT and the 4p-IpDFT algorithms proposed in [18] and [12]. Accuracies comparison with two state-of-the-art multi-point algorithms is performed in Section 4 through computer simulations considering either noisy and noisy and harmonically distorted damped sinusoids. Some conclusions are finally presented in Section 5.

2. Analysis of the generalized multi-point IpDTFT algorithm

The analyzed discrete-time noisy damped sinusoid, obtained by a sampling with rate f_s a continuous-time noisy damped sinusoid, is expressed as:

$$\begin{aligned} y(m) &= A\mathrm{e}^{-\frac{1}{f_s}\beta m}\cos\left(2\pi\frac{f}{f_s}m+\phi\right)+\zeta(m) \\ &= A\mathrm{e}^{-\frac{2\pi}{M}\alpha m}\cos\left(2\pi\frac{\vartheta}{M}m+\phi\right)+\zeta(m)=x(m)+\zeta(m), m \\ &= 0,1,2,\cdots,M-1 \end{aligned} \tag{1}$$

where $x(\bullet)$ is the noise free damped sinusoid of amplitude A, frequency f, phase ϕ, and damping factor β, while $\zeta(\bullet)$ is an additive white Gaussian noise with zero mean and variance σ_n^2. M is the acquisition length. The Signal-to-Noise Ratio (SNR) of the signal (1) is defined as $SNR=\frac{A^2}{2\sigma^2}$. In (1) $\vartheta \triangleq M\frac{f}{f_s}$ and $\alpha \triangleq \frac{M}{2\pi}\frac{\beta}{f_s}$ represents the normalized frequency and the normalized damping factor, respectively. Their definition enables the achievement of simple expressions for the related IpDTFT estimators.

The normalized frequency represents the number of analysed signal cycles, and it can be expressed as:

$$\vartheta = l+\delta, \tag{2}$$

where l is the rounded value of ϑ, and δ ($-0.5 \le \delta < 0.5$) is the rounding error, which corresponds to the inter-bin frequency location; $\delta = 0$ if coherent sampling occurs. The value of l is usually estimated as the location of the peak of the squared DFT module [5,8,15]. Thus, the frequency estimation problem can be solved by determining the fractional frequency δ.

To reduce the spectral leakage contribution due to the fundamental image component (and possible spurious components) on the frequency and the damping factor estimates, the acquired signal is multiplied by the H-term MSD window defined as:

$$w(m)=\sum_{h=0}^{H-1}(-1)^h a_h\cos\left(\frac{2\pi hm}{M}\right), m=0,1,\cdots,M-1 \tag{3}$$

where $a_0=\frac{C_{2H-2}^{H-1}}{2^{2H-2}}$ and $a_h=\frac{C_{2H-2}^{H-1-h}}{2^{2H-3}}$, $h=1,2,\cdots,H-1$, with $C_n^k=\frac{n!}{(n-k)!\bullet k!}$ are the window coefficients [25]. Thus, the analyzed signal becomes $y_w(m)=y(m)\bullet w(m)$.

The DTFT of the noise free weighted damped sinusoid $x_w(m)=x(m)\bullet w(m)$, is given by:

$$\begin{aligned} X_w(\lambda) &= \frac{A}{2}W\left(\mathrm{e}^{\frac{2\pi}{M}(\alpha+\mathrm{j}(\lambda-\vartheta))}\right)\mathrm{e}^{\mathrm{j}\phi}+\frac{A}{2}W\left(\mathrm{e}^{\frac{2\pi}{M}(\alpha+\mathrm{j}(\lambda+\vartheta))}\right)\mathrm{e}^{-\mathrm{j}\phi} \\ &= \widetilde{X}_w(\lambda)+\widetilde{X}_{iw}(\lambda),\ \lambda\in\left[0,\frac{M}{2}\right), \end{aligned} \tag{4}$$

where

$$W\left(\mathrm{e}^{\frac{2\pi}{M}(\alpha+\mathrm{j}\nu)}\right) \cong \frac{(2H-2)!}{2^{2H-1}}\frac{M}{\pi}\frac{1-\mathrm{e}^{-2\pi(\alpha+\mathrm{j}\nu)}}{\alpha+\mathrm{j}\nu}\frac{1}{\prod_{h=1}^{H-1}\left[(\alpha+\mathrm{j}\nu)^2+h^2\right]}, \tag{5}$$

is the z-transform of (3) [15], while $\widetilde{X}_w(\lambda)$ and $\widetilde{X}_{iw}(\lambda)$ are the transforms of the fundamental component of $x_w(m)$ and of its image, respectively. The related expressions can be written as:

$$\widetilde{X}_w(\lambda) \cong \psi(\alpha+\mathrm{j}(\lambda-\vartheta))\mathrm{e}^{\mathrm{j}\phi}, \lambda\in[0,M/2), \tag{6.a}$$

$$\widetilde{X}_{iw}(\lambda) \cong \psi(\alpha+\mathrm{j}(\lambda+\vartheta))\mathrm{e}^{-\mathrm{j}\phi}, \lambda\in[0,M/2), \tag{6.b}$$

where;

$$\psi(\theta)\overset{\mathrm{def}}{=}\frac{(2H-2)!}{2^{2H}}\frac{AM}{\pi}\frac{1-\mathrm{e}^{-2\pi\theta}}{\theta\prod_{h=1}^{H-1}\left(\theta^2+h^2\right)}, \tag{7}$$

where θ is a complex-valued variable used to represent either $\alpha+\mathrm{j}(\lambda-\vartheta)$ or $\alpha+\mathrm{j}(\lambda+\vartheta)$.

The inter-bin frequency location and the damping factor can be estimated by the following generalized multi-point interpolation function:

$$h_r=\widehat{\delta}-r+\mathrm{j}\widehat{\alpha}=\frac{\sum_{p=-K_1}^{K_1}a_pY_w(l+r+p)}{\sum_{q=-K_2}^{K_2}b_qY_w(l+r+q)}, \tag{8}$$

where K_1 and K_2 are integers, $\{a_p\}$ $p=-K_1,-K_1+1,\ldots,K_1$, and $\{b_q\}$, q

$= -K_2, -K_2+1,\ldots, K_2$, are set of integers of integers, r $(-1 < r < 1)$ is a real-valued fractional frequency shift, and $Y_w(\bullet)$ is the DTFT of the windowed version of signal (1). The variable r acts as a tuning parameter and its value can be selected so to optimize the accuracy of the frequency and the damping factor estimates returned by (8). Observe that (8) is a ratio of two linear combinations of DTFT samples taken one bin apart and located around the index l of the discrete spectrum peak. Observe also that, with a suitable choice of the values of the coefficients, (8) can express different IpDTFT algorithms proposed in the literature [3,5,12,18].

The following Theorem holds (see the proof in the Appendix A):

Theorem. *When the analyzed damped sinusoid is weighted by the H-term MSD window, the contributions of the fundamental image component on the inter-bin frequency and damping factor estimators* (8) *are:*

$$\Delta\delta + \mathrm{j}\Delta\alpha \cong -2(l+\delta)\frac{\delta - r + \mathrm{j}\alpha}{-(\delta+2l+r)+\mathrm{j}\alpha}\frac{f(\alpha+\mathrm{j}(2l+\delta+r))}{f(\alpha-\mathrm{j}(\delta-r))}\mathrm{e}^{-\mathrm{j}2\phi}, \tag{9.a}$$

$$\Delta\delta + \mathrm{j}\Delta\alpha \cong -2(l+\delta)\frac{g(\alpha+\mathrm{j}(2l+\delta+r))}{g(\alpha-\mathrm{j}(\delta-r))}\mathrm{e}^{-2\mathrm{j}\phi}, \tag{9.b}$$

where $f(\nu) \stackrel{\text{def}}{=} \sum_{p=-K_1}^{K_1} a_p \psi(\nu+\mathrm{j}p)$ *and* $g(\nu) \stackrel{\text{def}}{=} \sum_{q=-K_2}^{K_2} b_q \psi(\nu+\mathrm{j}q)$.

Either (9.a) or (9.b) can be used for the computation of the fundamental image component contributions. In practice the choice of the expression to be used depends on the analytical complexity of the functions $f(\bullet)$ or $g(\bullet)$ in the specific case at hand. From (9) it follows that the estimation errors $\Delta\delta$ and $\Delta\alpha$ are two almost equal amplitude, in quadrature sinusoids with respect to the signal phase ϕ. Moreover, simulations show that the error amplitude decreases as ϑ increases.

The above Theorem enables the compensation of the image component contribution, so that an improved accuracy IpDTFT algorithm can be defined, whose application is advantageous especially when a few signal cycles are acquired. For a generic, but known, value of the fractional frequency shift r, that new algorithm, hereafter called corrected IpDTFT (IpDTFTc) algorithm, requires to perform the following steps:

Multi-point IpDTFTc algorithm:

Step 1: acquire M samples of the signal y(m)
Step 2: compute the DFT of the windowed signal $y_w(m) = y(m) \bullet w(m)$, *where w(m) is the H-term MSD window*
Step 3: determine the integer part l of the number of acquired signal cycles as the location of the peak of the DFT squared module
Step 4: determine an initial estimate for the inter-bin frequency location and the damping factor by applying (8) with a predefined value of r: $\widehat{\delta} = r + Re\{h_r\}$ and $\widehat{\alpha} = Im\{h_r\}$.
Step 5: compute $\widehat{\phi} = angle\left\{\frac{(\widehat{\alpha}-\mathrm{j}(\widehat{\delta}-r))\prod_{h=1}^{H-1}\left[(\widehat{\alpha}-\mathrm{j}(\widehat{\delta}-r))^2+h^2\right]}{1-\mathrm{e}^{-2\pi(\widehat{\alpha}-\mathrm{j}(\widehat{\delta}-r))}}Y_w(l)\right\}$, *which is derived from (4) and (5) by neglecting the contribution of the image component in (4)*
Step 6: determine the estimation errors $\Delta\delta$ *and* $\Delta\alpha$ *by applying (9) using the obtained estimates for* $\widehat{\alpha}$, $\widehat{\delta}$, *and* $\widehat{\phi}$
Step 7: compute the compensated estimates $\widehat{\delta}_c = \widehat{\delta} - \Delta\delta$ and $\widehat{\alpha}_c = \widehat{\alpha} - \Delta\alpha$.

Simulations showed that the *RMSE* of the parameters estimated by the IpDTFTc algorithm depends on the value of the fractional frequency shift r and that there exists a specific value $\widetilde{r}$ for which the *RMSE* of both unknown parameters reach a minimum. Simulation results showed that the optimum value of r is such that the processed DTFT samples are located symmetrically with respect to the normalized signal frequency ϑ. Thus, it depends on the fractional frequency δ and the adopted interpolation function (8), while it is almost independent of the damping factor α. It was determined *a-priori* by simulations, so that an optimal IpDTFTc (IpDTFTc-o) algorithm can be implemented as follows.

Multi-point IpDTFTc-o algorithm:

Steps 1–3: the same as Steps 1–3 of the IpDTFTc algorithm
Step 4: determine an initial estimate for the inter-bin frequency location by applying (8) with r = 0: $\widehat{\delta} = Re\{h_r\}$.
Step 5: determine a new estimate for the inter-bin frequency location and the damping factor by applying (8) with $r = \widetilde{r}$: $\widetilde{\delta} = \widetilde{r} + Re\{h_{\widetilde{r}}\}$ and $\widetilde{\alpha} = Im\{h_{\widetilde{r}}\}$.
Step 6: compute $\widetilde{\phi} = angle\left\{\frac{(\widetilde{\alpha}-\mathrm{j}(\widetilde{\delta}-\widetilde{r}))\prod_{h=1}^{H-1}\left[(\widetilde{\alpha}-\mathrm{j}(\widetilde{\delta}-\widetilde{r}))^2+h^2\right]}{1-\mathrm{e}^{-2\pi(\widetilde{\alpha}-\mathrm{j}(\widetilde{\delta}-\widetilde{r}))}}Y_w(l)\right\}$, *which is derived from (4) and (5) by neglecting the contribution of the image component in (4).*
Step 7: determine the estimation errors $\Delta\delta$ *and* $\Delta\alpha$ *by applying (9) using the obtained estimates for* $\widetilde{\alpha}$, $\widetilde{\delta}$, *and* $\widetilde{\phi}$.
Step 8: compute the compensated estimates $\widetilde{\delta}_c = \widetilde{\delta} - \Delta\delta$ and $\widetilde{\alpha}_c = \widetilde{\alpha} - \Delta\alpha$.

It is worth noticing that any value for the parameter r $(-1 \le r \le 1)$ can be used in Step 4. The value $r = 0$ is proposed since in this case the DTFT samples involved in (8) have been already computed in Step 2, so reducing the required processing effort.

3. The three-point and four-point IpDTFTc-o algorithms

In this Section the theory developed in Section 2 is applied to both the 3p-IpDFT algorithm proposed in [18] and the 4p-IpDFT algorithm proposed in [12]. The MSD windows are considered.

3.1. The three-point IpDTFTc-o algorithm

Assuming $K_1 = 1$, $K_2 = 1$, $a_{-1} = -H$, $a_0 = 0$, $a_1 = H$, $b_{-1} = 1$, $b_0 = -2$, and $b_1 = 1$, the generalized interpolation function (8) becomes:

$$\widehat{\delta} - r + \mathrm{j}\widehat{\alpha} = H\frac{Y_w(l+r+1) - Y_w(l+r-1)}{Y_w(l+r-1) - 2Y_w(l+r) + Y_w(l+r+1)}. \tag{10}$$

In particular, when $r = 0$ the 3p-IpDFT algorithm based on the *H*-term MSD window is obtained [18,22–24].

By using (4) and (6), after some algebra it follows that:

$$g(\nu) = -\frac{2H(2H-1)}{\nu^2+H^2}\psi(\nu). \tag{11}$$

By replacing (11) in (9.b) and exploiting (7) it results:

$$\Delta\delta + j\Delta\alpha \cong -2(l+\delta)\frac{1-\mathrm{e}^{-2\pi(\alpha+\mathrm{j}(\delta+r))}}{1-\mathrm{e}^{-2\pi(\alpha-\mathrm{j}(\delta-r))}}\frac{\alpha-\mathrm{j}(\delta-r)}{\alpha+\mathrm{j}(2l+\delta+r)}\frac{\prod_{h=1}^{H}\left[(\alpha-\mathrm{j}(\delta-r))^2+h^2\right]}{\prod_{h=1}^{H}\left[(\alpha+\mathrm{j}(2l+\delta+r))^2+h^2\right]}\mathrm{e}^{-2\mathrm{j}\phi}. \tag{12}$$

Fig. 1 shows the values of the estimation errors $\Delta\delta$ and $\Delta\alpha$ obtained through simulations and by applying (12) for the 3p-IpDTFT algorithm as a function of the signal phase ϕ when $r = -0.2$ and $r = 0.5$. The signal phase varies in the range [0, 2π) rad with a step of π/20 rad and a noise free damped sinusoid with $A = 1$ p.u., $\vartheta = 3.3$ cycles and $\alpha = 0.5$ is considered. Both the rectangular and the two-term MSD (or Hann) windows are used, and $M = 512$ samples are processed. As we can see, simulation and theoretical results are very close to each other. Also, the estimation errors related to the Hann window are smaller due to the lower spectrum sidelobe level of that window. It is worth noticing that the same behaviour as in Fig. 1 is achieved when the frequency shift $r \in (-1, 1)$, the damping factor $\alpha \in (0, 2)$, and $M \ge 64$ samples.

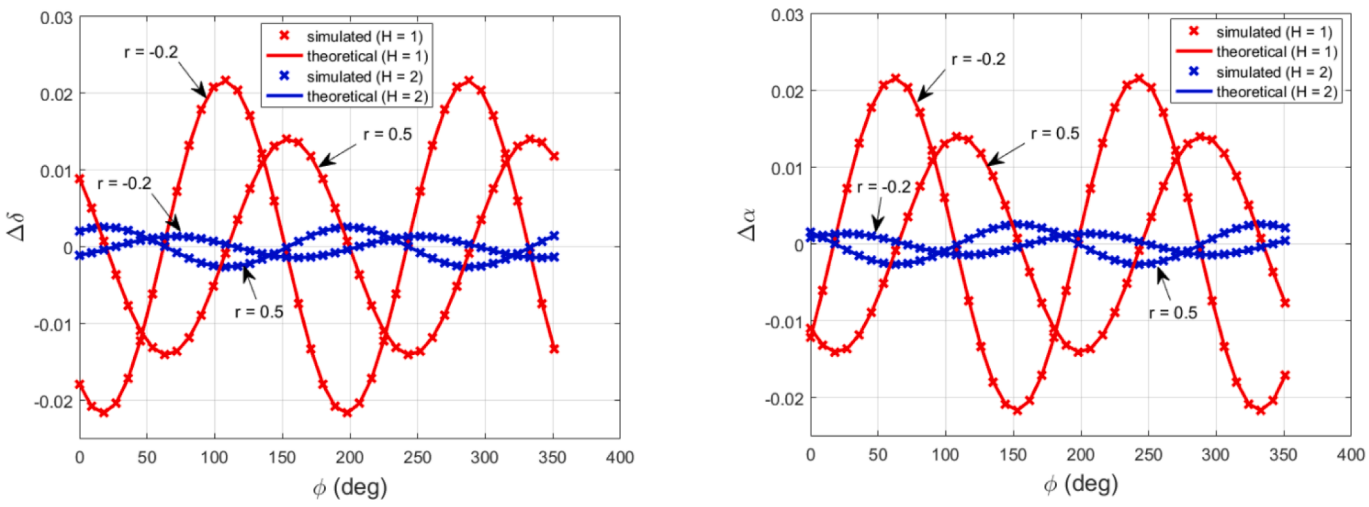

Fig. 1. Pure damped sinusoid: estimation errors $\Delta\delta$ (a) and $\Delta\alpha$ (b) obtained through simulations and (12) for the 3p-IpDTFT algorithm versus the signal phase when $r = -0.2$ and $r = 0.5$. Sinusoid amplitude $A = 1$ p.u., $\vartheta = 3.3$ cycles, damping factor $\alpha = 0.5$, $M = 512$ samples. The rectangular or the Hann windows are applied.

For the 3p-IpDTFTc-o algorithm, performed simulations showed that the optimal value $\widetilde{r}$ of the fractional shift is equal to the estimate $\widehat{\delta}$ returned by the 3p-IpDTFT algorithm. For example, the Root Mean Square Errors (*RMSEs*) of the inter-bin frequency and damping factor estimates returned by the 3p-IpDTFTc and the 3p-IpDTFTc-o algorithms based on the rectangular and the Hann windows are reported in Fig. 2 as a function of r, which varies in the range $(-1, 1)$ with a step of 0.1. The number of cycles of the analyzed noisy damped sinusoids is equal to $\vartheta = 3.6$ or 4.4 cycles when the rectangular window is considered, and $\vartheta = 2.6$ or 3.4 cycles when the Hann window is applied. The damped sinusoid amplitude is $A = 1$ p.u., the damping factor is $\alpha = 0.5$, and $SNR = 40$ dB; 10,000 runs of $M = 512$ samples acquired with signal phase at random have been processed for each value of r. Fig. 2 confirms that, for both windows, the inter-bin frequency and the damping factor estimates achieve minimum *RMSE* values when $\widetilde{r}$ is close to δ. The same result was returned by simulations when considering different observation signal lengths when ϑ is greater than 2 or 3 cycles for the Hann and the rectangular window, respectively. Under these constraints, the accuracy of the initial parameter estimates enables the 3p-IpDTFTc-o algorithm to provide high accuracy estimates, as shown in the following.

Fig. 3 shows the *RMSEs* of the parameters estimated by the 3p-IpDFT algorithm [18], the 3p-IpDTFTc algorithm with $r = -0.4$, $r = 0$, and $r = 0.4$, and the 3p-IpDTFTc-o algorithm as a function of the number of acquired signal cycles ϑ, which varies with a step of 0.1 cycles. A noisy damped sinusoids with $A = 1$ p.u., damping factor $\alpha = 0.5$ and $SNR = 40$ dB is considered. Both the rectangular (Fig. 3(a), (b)) and the Hann (Fig. 3(c), (d)) windows are applied. 10,000 runs of $M = 512$ samples have been performed for each value of ϑ by varying the signal phase at random.

Fig. 3 shows that the 3p-IpDTFTc algorithm applied with $r = -0.4$, 0, or 0.4 exhibits a minimum *RMSE* value when the selected value of r is close to δ. In addition, Fig. 3 shows that the 3p-IpDTFTc-o algorithm provides more accurate parameter estimates than the 3p-IpDFT algorithm [18], and the IpDTFTc algorithm applied using $r = -0.4$, 0, and 0.4 when ϑ is greater than about 2 or 3 cycles for the Hann or the rectangular window, respectively. Specifically, under the above constraints, the IpDTFTc-o algorithm provides the minimum estimation *RMSEs* ensured by the IpDTFTc algorithm.

Conversely, for short observations (i.e., ϑ smaller than 2 or 3 cycles, respectively), the 3p-IpDTFTc algorithm applied with $r = 0.4$ may exhibit a bit better accuracy than the 3p-IpDTFTc-o algorithm. That behaviour occurs since in these conditions the accuracy of the initial parameter estimates returned by the 3p-IpDTFTc algorithm is poor due to the significant contribution of the fundamental image component.

It is also worth remarking that, when at least about 2 or 3 cycles are analysed in the case of the Hann or the rectangular window, respectively, the *RMSE* values returned by the IpDTFTc-o algorithm are almost constant since the effect of wideband noise largely prevails over the interference from the fundamental image component, which is well compensated by the algorithm. Conversely, *RMSE* fluctuations occur if the 3p-IpDTFTc algorithm is adopted due to both the effect of noise and the residual contribution of the fundamental image component. *RMSE* behaviors very similar to those reported in Fig. 3 were obtained by applying the IpDTFTc algorithm using different values of the fractional shift r in the range $(-1, 1)$.

Fig. 4 shows the *RMSEs* of the parameters estimated by the 3p-IpDFT algorithm, the 3p-IpDTFTc algorithm applied with $r = -0.4$, 0, or 0.4, and the 3p-IpDTFTc-o algorithm as a function of the damping factor α, which varies in the range [0.05, 2] with a step of 0.05; $\vartheta = 3.3$ cycles are processed. The remaining simulation parameters are like those in Fig. 3.

The obtained results confirm those obtained in Fig. 3 when $\vartheta = 3.3$ cycles. Moreover, the *RMSEs* of the unknown parameters increase as the damping factor α increases.

3.2. The four-point IpDTFTc-o algorithm

A 4p-IpDFT algorithm based on the rectangular window has been proposed in [12]. The following Proposition extends that algorithm to the MSD windows (see the proof in the Appendix B).

Proposition. *A 4p-IpDFT estimator for the frequency and the damping*

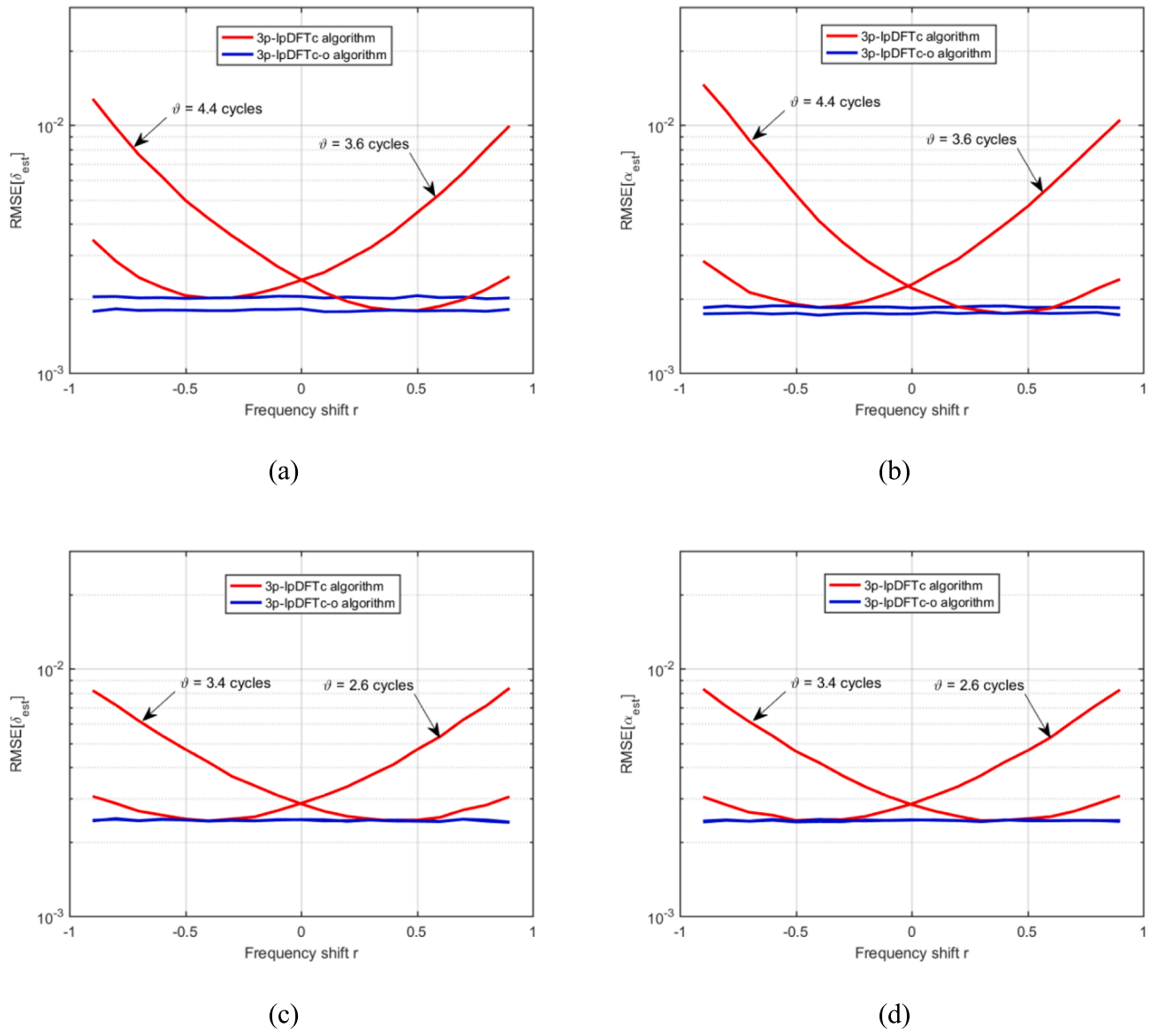

Fig. 2. Noisy damped sinusoids: simulation results for the *RMSE*s of the inter-bin frequency and the damping factor estimators returned by the generalized 3p-IpDTFTc and the 3p-IpDTFTc-o algorithms versus the fractional frequency shift *r*. Rectangular window (a), (b) and Hann window (c), (d). Sinusoid amplitude $A = 1$ p.u., damping factor $\alpha = 0.5$, and $SNR = 40$ dB. $\vartheta = 3.6$ and 4.4 cycles (a), (b) and $\vartheta = 2.6$ and 3.4 cycles (c), (d). 10,000 runs of $M = 512$ samples each with signal phase chosen at random.

factor of a damped sinusoid based on the H-term MSD window can be obtained by the following expression:

$$h=\widehat{\delta}+\mathrm{j}\widehat{\alpha}=\frac{-(H+1)Y_w(l-2)+(H+2)Y_w(l-1)+(H-1)Y_w(l)-HY_w(l+1)}{Y_w(l-2)-3Y_w(l-1)+3Y_w(l)-Y_w(l+1)}. \tag{13}$$

The estimator (13) can be obtained as a particular case of (8) assuming $r = 0$, $K_1 = 2$, $K_2 = 2$,$a_{-2} = -(H + 1)$, $a_{-1} = H + 2$, $a_0 = H - 1$, $a_1 = -H$, $a_2 = 0$, $b_{-2} = 1$, $b_{-1} = -3$, $b_0 = 3$, $b_1 = -1$, and $b_2 = 0$. The related generalized interpolation function (8) is:

From (B.3.b) it follows that:

$$g(\nu) = -\frac{2H(4H^2-1)\mathrm{j}}{(\nu^2+H^2)(\nu-j(H+1))}\psi(\nu). \tag{15}$$

By replacing (15) in (9.b) and exploiting (7) it results:

$$h_r=\widehat{\delta}-r+\mathrm{j}\widehat{\alpha}=\frac{-(H+1)Y_w(l+r-2)+(H+2)Y_w(l+r-1)+(H-1)Y_w(l+r)-HY_w(l+r+1)}{Y_w(l+r-2)-3Y_w(l+r-1)+3Y_w(l+r)-Y_w(l+r+1)}. \tag{14}$$

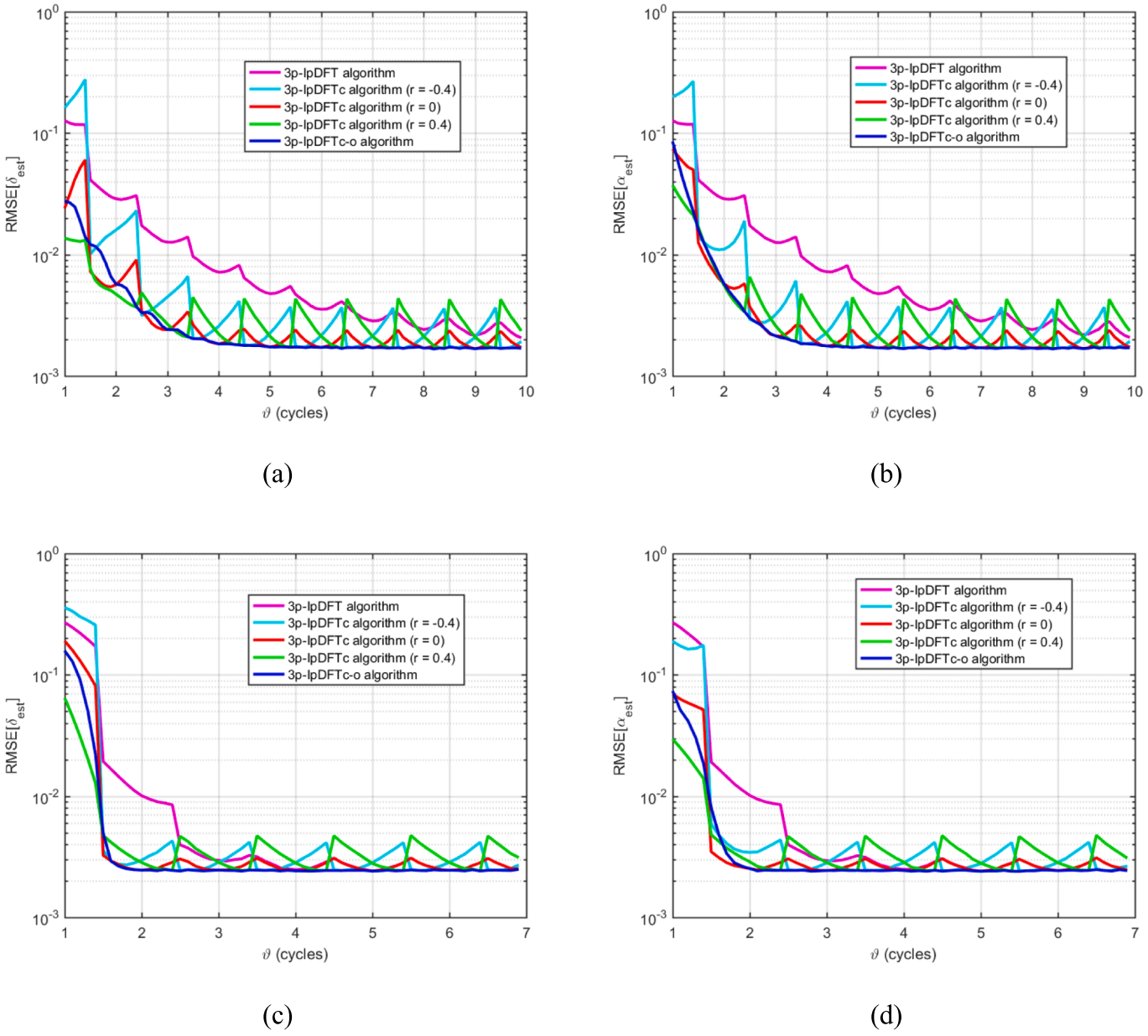

Fig. 3. Noisy damped sinusoids: simulation results for the *RMSEs* of the inter-bin frequency and the damping factor estimators provided by the 3p-IpDFT algorithm [18], the generalized 3p-IpDTFTc algorithm with $r = -0.4$, 0, or 0.4, and the 3p-IpDTFTc-o versus the number of analyzed cycles. Rectangular window (a), (b) and Hann window (c), (d). Sinusoid amplitude $A = 1$ p.u., damping factor $\alpha = 0.5$, and $SNR = 40$ dB. 10,000 runs of $M = 512$ samples each with signal phase chosen at random.

$$\Delta\delta + j\Delta\alpha \cong -2(l+\delta)\frac{1-e^{-\pi(\alpha+j(\delta+r))}}{1-e^{-\pi(\alpha-j(\delta-r))}} \frac{(\alpha-j(\delta-r))(\alpha-j(\delta-r)-j(H+1))}{(\alpha+j(2l+\delta+r))(\alpha+j(2l+\delta+r)-j(H+1))} \times \frac{\prod_{h=1}^{H}\left[(\alpha-j(\delta-r))^2+h^2\right]}{\prod_{h=1}^{H}\left[(\alpha+j(2l+\delta+r))^2+h^2\right]} e^{-2j\phi}. \quad (16)$$

Fig. 5 shows the values of the estimation errors $\Delta\delta$ and $\Delta\alpha$ obtained through simulations and (16) for the 4p-IpDTFT algorithm as a function of the signal phase ϕ. The simulation parameters are the same as in Fig. 1 and the rectangular or the two-term MSD windows are adopted. As expected, simulation and theoretical results are very close to each other. It is worth noticing that behaviours similar to those reported in Fig. 5 are achieved when the frequency shift $r \in (-1, 1)$, the damping factor $\alpha \in (0, 2)$, and at least $M = 32$ samples are analysed.

In the 4p-IpDTFTc-o algorithm, the value $\tilde{r}$ selected for the fractional shift is equal to $0.5 + \hat{\delta}$, which almost corresponds to the minimum *RMSE* values, as shown in Fig. 6, in which the *RMSEs* of the inter-bin frequency and the damping factor estimates returned by the 4p-IpDTFTc and 4p-IpDTFTc-o algorithms are reported as a function of r. Both the rectangular and Hann windows are considered, and the signal parameters are the same used in Fig. 2.

In Fig. 6 clearly shows that, for both windows, the minimum *RMSE* values of the inter-bin frequency and the damping factor estimates are obtained when $\tilde{r}$ is close to $0.5 + \delta$. The same result was obtained when considering different observation signal lengths if ϑ is greater than about 1.9 or 2.6 cycles when the Hann or the rectangular window are applied, respectively. Under these constraints, the accuracy of the initial parameter estimates enables the 4p-IpDTFTc-o algorithm to return high accuracy estimates, as shown in the following.

Fig. 7 shows the *RMSEs* of the parameters estimated by the 4p-IpDFT

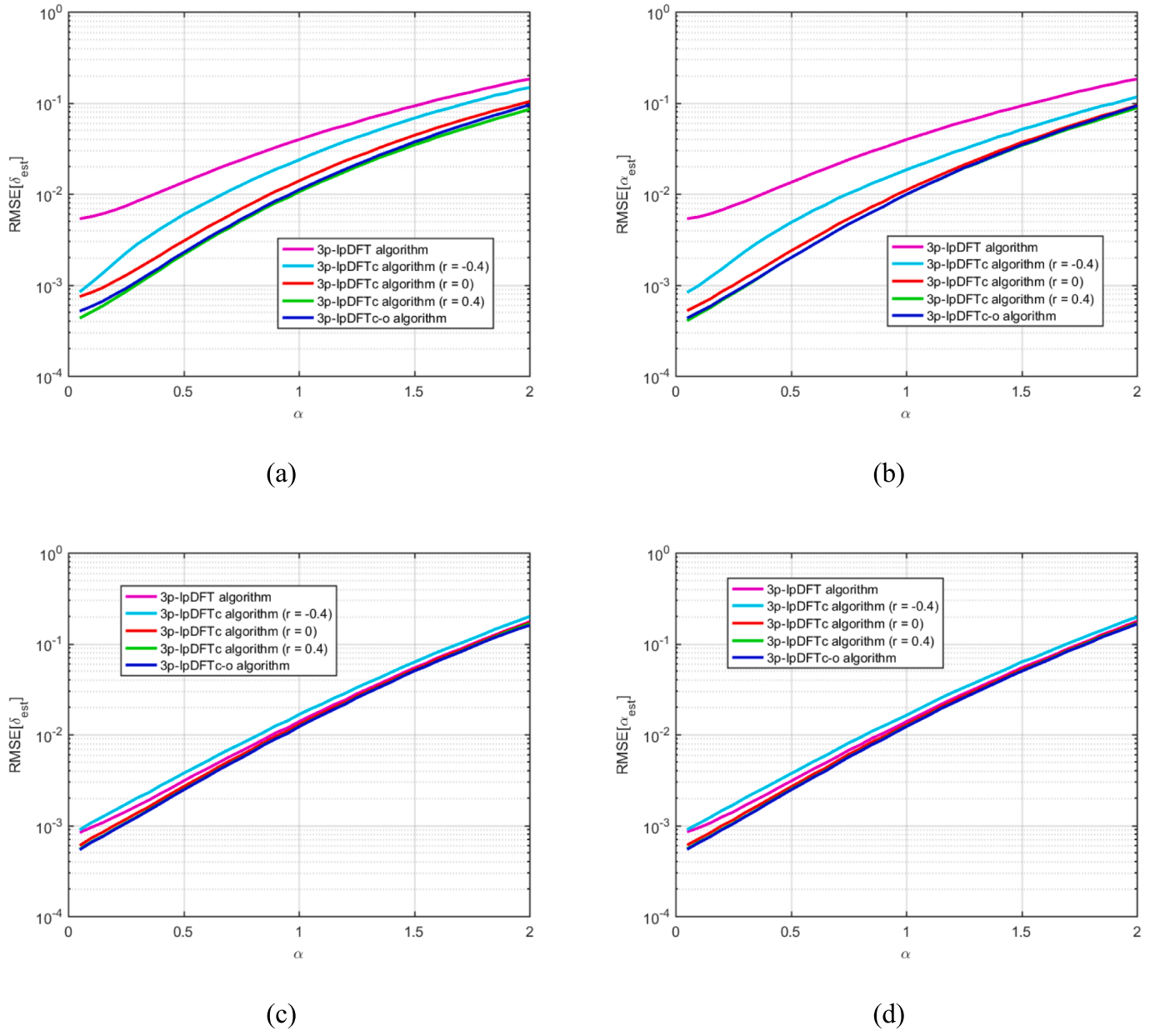

Fig. 4. Noisy damped sinusoids: simulation results for the RMSEs of the inter-bin frequency and the damping factor estimators provided by the 3p-IpDFT algorithm [18], the generalized 3p-IpDTFTc algorithm with $r = -0.4$, 0, or 0.4, and the 3p-IpDTFTc-o versus the damping factor. Rectangular window (a), (b) and Hann window (c), (d). Sinusoid amplitude $A = 1$ p.u., number of analyzed cycles $\vartheta = 3.3$ cycles, and $SNR = 40$ dB. 10,000 runs of $M = 512$ samples each with signal phase chosen at random.

algorithm (13), the IpDTFTc algorithm applied with $r = -0.4$, $r = 0$, and $r = 0.4$, and the 4p-IpDTFTc-o algorithm as a function of the number of acquired signal cycles ϑ, which varies with a step of 0.1 cycles. Both the rectangular (Fig. 7(a), (b)) and the Hann (Fig. 7(c), (d)) windows are applied and the same simulation parameters as in Fig. 3 are considered. Observe that at least 2 signal cycles have been considered in order to ensure that the frequencies related to all the DTFT samples appearing in (13) are positive. As we can see, the 4p-IpDTFTc algorithm provides the minimum estimate *RMSE* values for both considered windows when r is close to $0.5 + \delta$. Also, Fig. 7 shows that the proposed 4p-IpDTFTc-o algorithm outperforms the others in almost all considered situations. As expected, the 4p-IpDTFTc algorithm with $r = 0$ exhibits a better accuracy than the 4p-IpDFT algorithm (13) only when a few signal cycles ϑ are analyzed. Moreover, the 4p-IpDTFTc-o algorithm ensures almost constant *RMSE* values when at least about 3 or 2 cycles are observed and the rectangular or the Hann windows are employed, respectively. Simulations confirm that these values coincide with the minima of the estimation *RMSE* provided by the IpDTFTc algorithms for different values of the fractional shift r in the range $(-1, 1)$. It is also worth remarking that the variations of the *RMSE* returned by the 4p-IpDTFTc algorithm when ϑ is greater than about 2 or 3 cycles and the Hann or the rectangular window is used, respectively, are due to both the effect of noise and the residual contribution of the fundamental image component.

Fig. 8 shows the *RMSEs* of the parameters estimated by the 4p-IpDFT algorithm (13), the 4p-IpDTFTc algorithm with $r = -0.4$, 0, or 0.4, and the 4p-IpDTFTc-o algorithm as a function of the damping factor α, which varies in the range [0.05, 2] with a step of 0.05, when $\vartheta = 3.3$ cycles. The

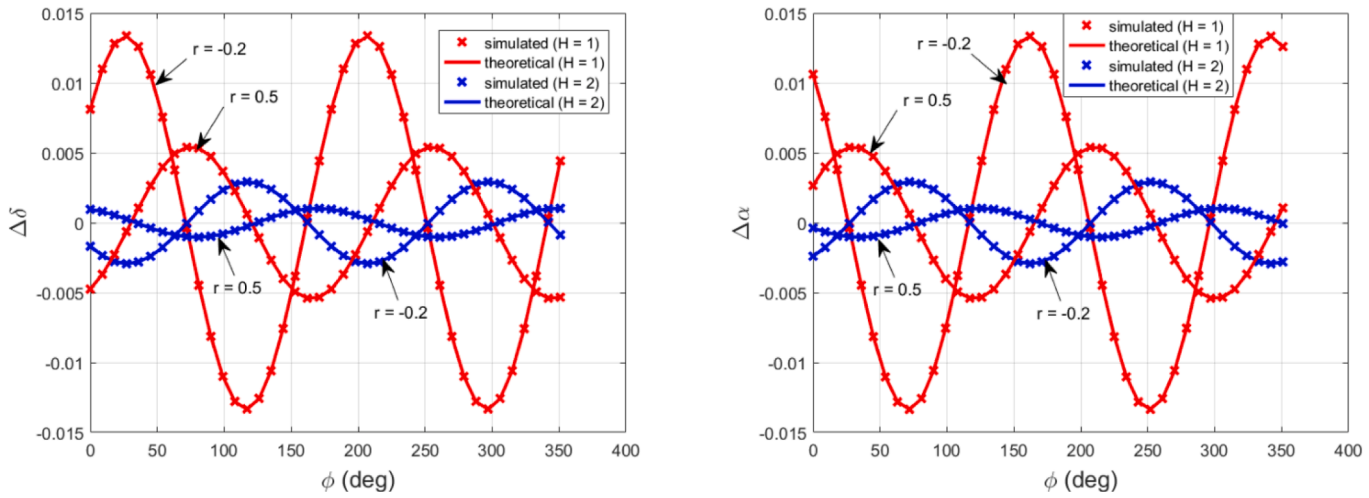

Fig. 5. Pure damped sinusoid: estimation errors $\Delta\delta$ (a) and $\Delta\alpha$ (b) obtained through simulations and (16) for the 4p-IpDTFT algorithm versus the signal phase when $r = -0.2$ and $r = 0.5$. Sinusoid amplitude $A = 1$ p.u., $\vartheta = 3.3$ cycles, damping factor $\alpha = 0.5$, $M = 512$ samples. The rectangular or the Hann windows are applied.

same simulation parameters as in Fig. 3 have been used. As we can see, the *RMSE*s of the unknown parameters confirm the results obtained in Fig. 7 when $\vartheta = 3.3$ cycles and they increase with the damping factor α.

4. Performance comparison with state-of-the-art multi-point IpDTFT algorithms

In this Section the *RMSE* of the proposed 3p-IpDTFTc-o and 4p-IpDTFTc-o algorithms and the 3p-IpDTFT algorithms proposed in [3] and [16] are compared to each other through Monte Carlo simulations. The IpDTFT algorithm proposed in [16], already discussed in the Introduction and called here the Wang algorithm, is a 3p-IpDTFT algorithm based on the rectangular window and it removes the contribution of the fundamental image component on the returned estimates. The RVCI-1 algorithm proposed in [3] is a 3p-IpDFT algorithm based on the Hann window. Noisy damped sinusoids and noisy and harmonically distorted damped sinusoids are considered in the comparison. They are characterized by amplitude $A = 1$ p.u. and damping factor $\alpha = 0.5$. For each value of the number of cycles ϑ, 10,000 runs of $M = 512$ samples each are processed; the signal phase ϕ is selected at random in the interval $[0,2\pi)$ rad. Eventually, the processing efforts required by the most accurate of the considered algorithms are determined and compared with each other.

4.1. Noisy damped sinusoids

Fig. 9 shows the *RMSE*s of the inter-bin frequency and the damping factor estimates as a function of the number of analysed signal cycles ϑ in the case of damped sinusoids corrupted by noise so that the $SNR = 40$ dB (Fig. 9(a), (b)) or $SNR = 60$ dB (Fig. 9(c), (d)), respectively. The Wang algorithm, the RVCI-1 algorithm, and the proposed 3p-IpDTFTc-o algorithms based on the rectangular or the Hann windows are considered. The square root of the asymptotic Cramér-Rao Lower Bound (CRLB) for unbiased parameter estimators [26] is also shown in Fig. 9 in order to enable a visual assessment of the algorithm statistical efficiency.

As we can see, thanks to a more effective removal of the contribution of the fundamental image component, the Wang algorithm outperforms the others when a few signal cycles are observed. Indeed, in this situation the accuracies of the IpDTFTc-o algorithms suffer of the poor initial parameters estimates due to the strong contribution of the fundamental image component. Conversely, when the observation duration increases, the noise contribution dominates, and the IpDTFTc-o algorithm based on the rectangular window ensures the best accuracy. Good results are returned also by the IpDTFTc-o algorithm based on the Hann window, but the effect of noise on the estimated parameters increases due to the higher window equivalent noise bandwidth (*ENBW*) parameter. Simulations showed that the value of ϑ above which the IpDTFTc-o algorithm based on the rectangular window outperforms the others increases with the *SNR* and the damping factor. This behaviour occurs since for high *SNR* values the effect of the fundamental image component dominates also for relatively long observation intervals.

Moreover, estimation errors increase with the damping factor (as shown in Fig. 4) so longer observation intervals are needed to ensure that the effect of noise prevails. The RVCI-1 algorithm exhibits poor inter-bin frequency location accuracy when short observation intervals are analysed, and poor damping factor estimates. That occurs since this algorithm does not compensate the contribution of the fundamental image component. Fig. 9 also shows that the *RMSE* of the IpDTFTc-o algorithm based on the rectangular window is almost close to the CRLB if enough long observations are considered.

4.2. Noisy and harmonically distorted damped sinusoids

In the performed simulations the noisy signals considered in the previous subsection has been corrupted with a second and a third harmonics of amplitudes 0.1 p.u., 0.05 p.u., and damping factors 0.375, 0.25, respectively. Only low order harmonics were considered since their effect on the estimated parameters usually overcomes that due to the higher order ones [27].

Fig. 10 and Fig. 11 show the *RMSE*s of the inter-bin frequency and damping factor estimates returned by the Wang, the 3p-DTFTc-o, and the 4p-IpDTFTc-o algorithms based on the rectangular (Fig. 10) or the Hann (Fig. 11) windows as a function of the number of analyzed signal cycles ϑ when $SNR = 40$ dB or $SNR = 60$ dB. The square root of the asymptotic CRLB is also shown in order to provide a reference for the estimation accuracy.

As expected, the Wang algorithm is less robust to spectral interference from harmonics than the 3p-IpDTFTc-o and the 4p-IpDTFTc-o algorithms, which outperform the former algorithm in all considered simulation conditions, except when less than about 1.5 or 2.5 cycles are analysed and the rectangular or the Hann window are used, respectively. This occurs because the unknown parameter estimates are significantly

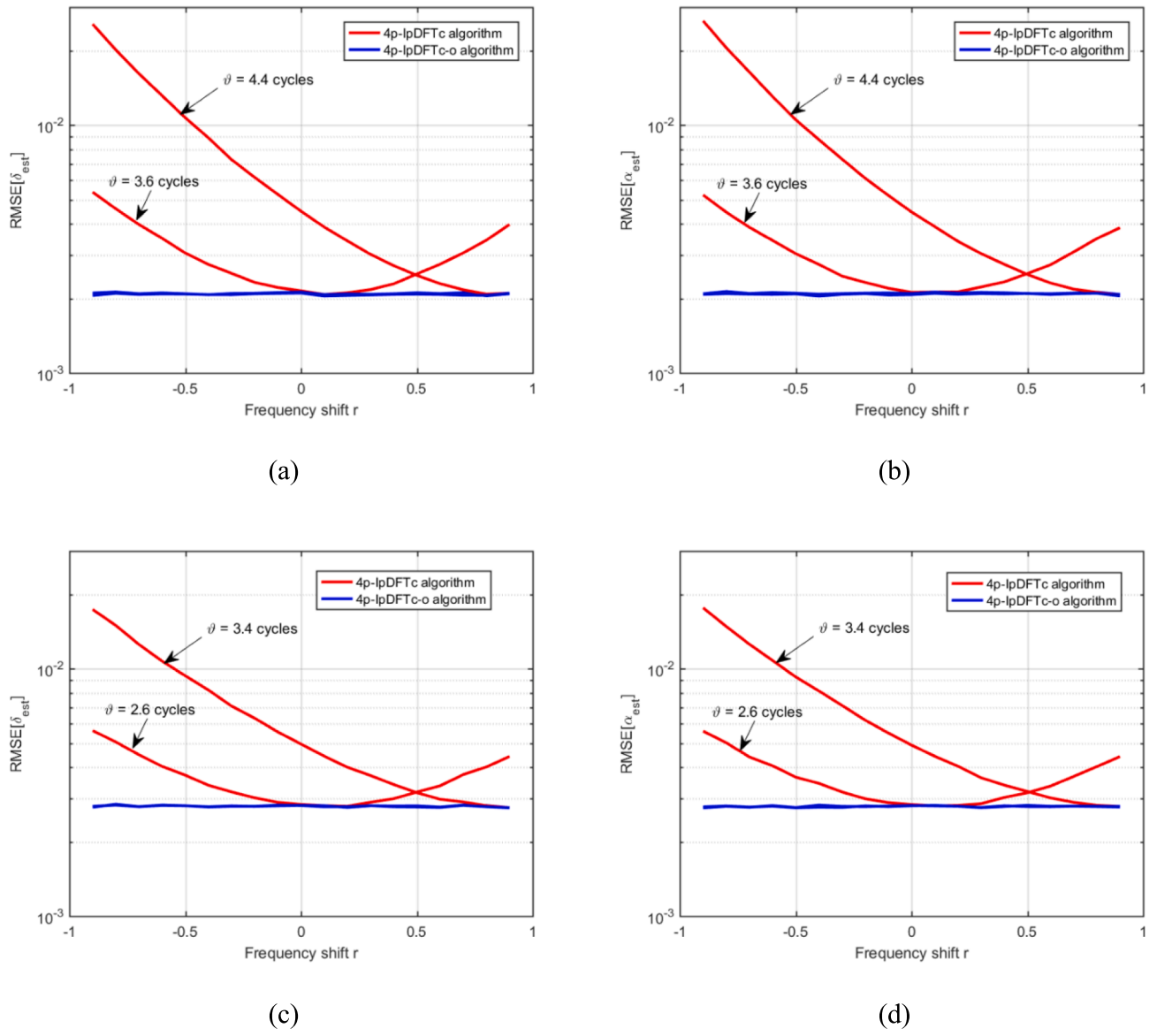

Fig. 6. Noisy damped sinusoids: simulation results for the *RMSE*s of the inter-bin frequency and the damping factor estimators returned by the generalized 4p-IpDTFTc and the 4p-IpDTFTc-o algorithms versus the fractional frequency shift *r*. Rectangular window (a), (b) and Hann window (c), (d). Sinusoid amplitude $A = 1$ p.u., damping factor $\alpha = 0.5$, and $SNR = 40$ dB. $\vartheta = 3.7$ and 4.3 cycles (a), (b) and $\vartheta = 2.7$ and 3.3 cycles (c), (d). 10,000 runs of $M = 512$ samples each with signal phase chosen at random.

affected by the interference from the harmonics, especially when the rectangular window is used. Observe also that the IpDTFTc-o algorithms outperforms the RVCI-1 algorithm in most considered conditions. When $SNR = 60$ dB, the 4p-IpDTFTc-o algorithm often outperforms the 3p-IpDTFTc-o algorithm if the rectangular window is used (see Fig. 10(c) and (d)), while their accuracies are very close when the Hann window is used. It is worth noticing that the unknown parameter *RMSE*s increase when the damping factors of the fundamental and harmonics increase. However similar behaviours as those in Figs. 10 and 11 are obtained if the damping factor ratios (i.e., 1:0.75:0.5) and the amplitude ratios are preserved.

4.3. Computational complexity comparison

The processing efforts required by the considered algorithms have been compared to each other. The number of analyzed sample *M* has been selected to be a power of 2 so that the classical FFT algorithm can be employed to determine the signal DFT by performing $Mlog_2M$ complex-valued additions and $0.5Mlog_2M$ complex-valued multiplications [28], which require $3Mlog_2M$ real-valued additions (RVAs) and $2Mlog_2M$ real-valued multiplications (RVMs). In all parameter estimators, the integer part of the number of analyzed signal cycles, *l*, is determined through a peak search procedure applied to the DFT square module, which implies *M* RVAs and 2*M* RVMs. The calculation of the DTFT of an *M*-length real-valued data sequence implies $(2M - 2)$ RVAs and 2 *M* RVMs. Further *M* RVMs are needed when data windowing is applied. The overall number of real-valued additions and multiplications required by the Wang, the 3p-IpDTFTc-o, and the 4p-IpDTFTc-o algorithms based on the rectangular window are reported in Table 1. The computational complexity required by further processing performed in each algorithm does not significantly affect the whole processing effort, so it is neglected.

Table 1 shows that the Wang algorithm requires a lower processing effort than the 3p-IpDTFTc-o and the 4p-IpDTFTc-o algorithms. For

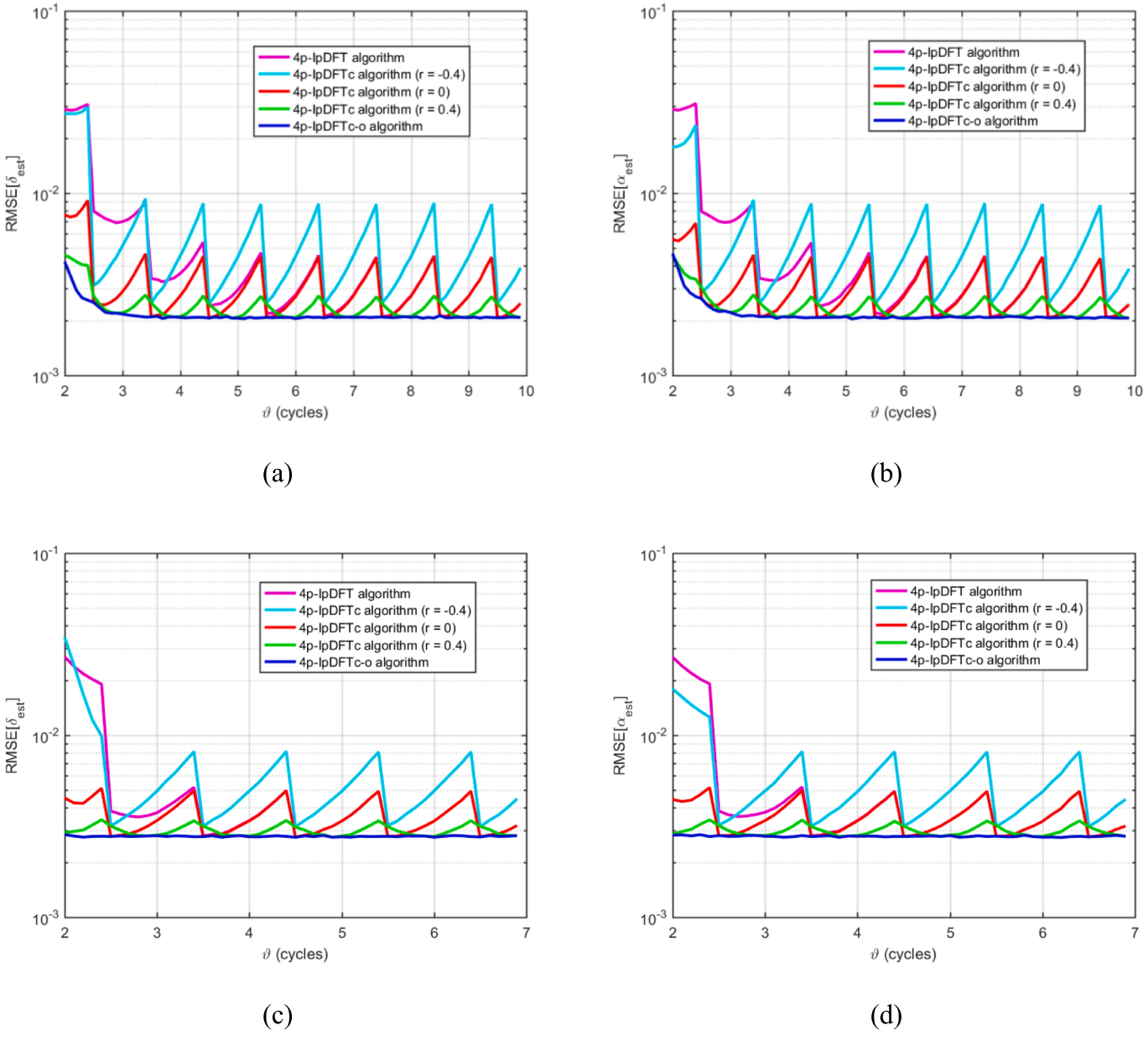

Fig. 7. Noisy damped sinusoids: simulation results for the *RMSE*s of the inter-bin frequency and the damping factor estimators provided by the 4p-IpDFT algorithm (13), the generalized 4p-IpDTFTc algorithm with $r = -0.4$, 0, or 0.4, the and 4p-IpDTFTc-o versus the number of analyzed cycles. Rectangular window (a), (b) and Hann window (c), (d). Sinusoid amplitude $A = 1$ p.u., damping factor $\alpha = 0.5$, and $SNR = 40$ dB. 10,000 runs of $M = 512$ samples each with signal phase chosen at random.

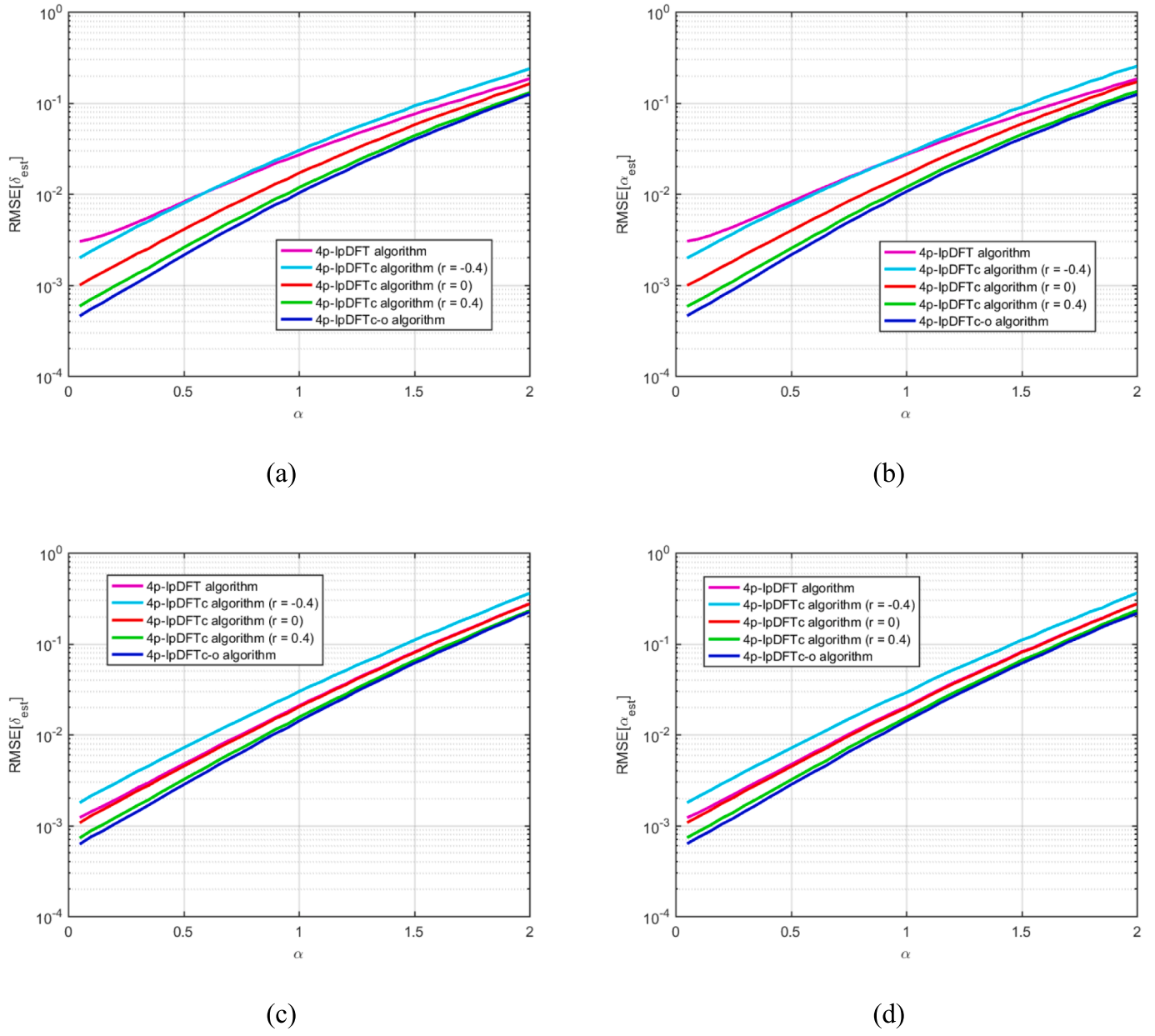

Fig. 8. Noisy damped sinusoids: simulation results for the *RMSE*s of the inter-bin frequency and the damping factor provided by the 4p-IpDTFTc-o versus the damping factor. Rectangular window (a), (b) and Hann window (c), (d). Sinusoid amplitude $A = 1$ p.u., number of analyzed cycles $\vartheta = 3.3$ cycles, and $SNR = 40$ dB. 10,000 runs of $M = 512$ samples each with signal phase chosen at random.

example, when $M = 512$ samples the 3p-IpDTFTc-o algorithm based on the rectangular window requires 21% more RVAs and 30% more RVMs than the Wang algorithm. However, the related processing effort is such that the IpDTFTc-o algorithm can surely implemented in most low-cost hardware platforms for real-time applications, thus ensuring significant advantages in terms of estimation accuracy when short observation intervals are of concern.

5. Conclusions

In this paper a generalized multi-point interpolated DTFT based on an MSD window has been proposed for frequency and damping factor estimation of real-valued damped sinusoids. The frequency-domain interpolation function is defined as the ratio between two generic linear combinations of DTFT samples located one bin apart, which is generalized exploiting a tuning parameter. Analytical expressions for the estimated parameter errors due to the interference of the fundamental image component have been derived. The obtained expressions enabled the compensation of that contribution and the derivation of a multi-point IpDTFT algorithm – called the IpDTFTc algorithm – which ensures a significant accuracy improvement when only a few signal cycles are analysed. In addition, a version of that algorithm – called the IpDTFTc-o algorithm – that provides minimum estimation *RMSE* has been proposed.

The developed theory has been applied to IpDTFT algorithms based on three or four interpolation points. Simulations showed that the proposed 3p-IpDTFTc-o and 4p-IpDTFTc-o algorithms can provide a better accuracy than state-of-the-art 3p-IpDFT estimators like the RVCI-1 [3] and the Wang [16] algorithms. Specifically, while the proposed IpDTFTc-o estimators outperforms the RVCI-1 algorithm, the Wang

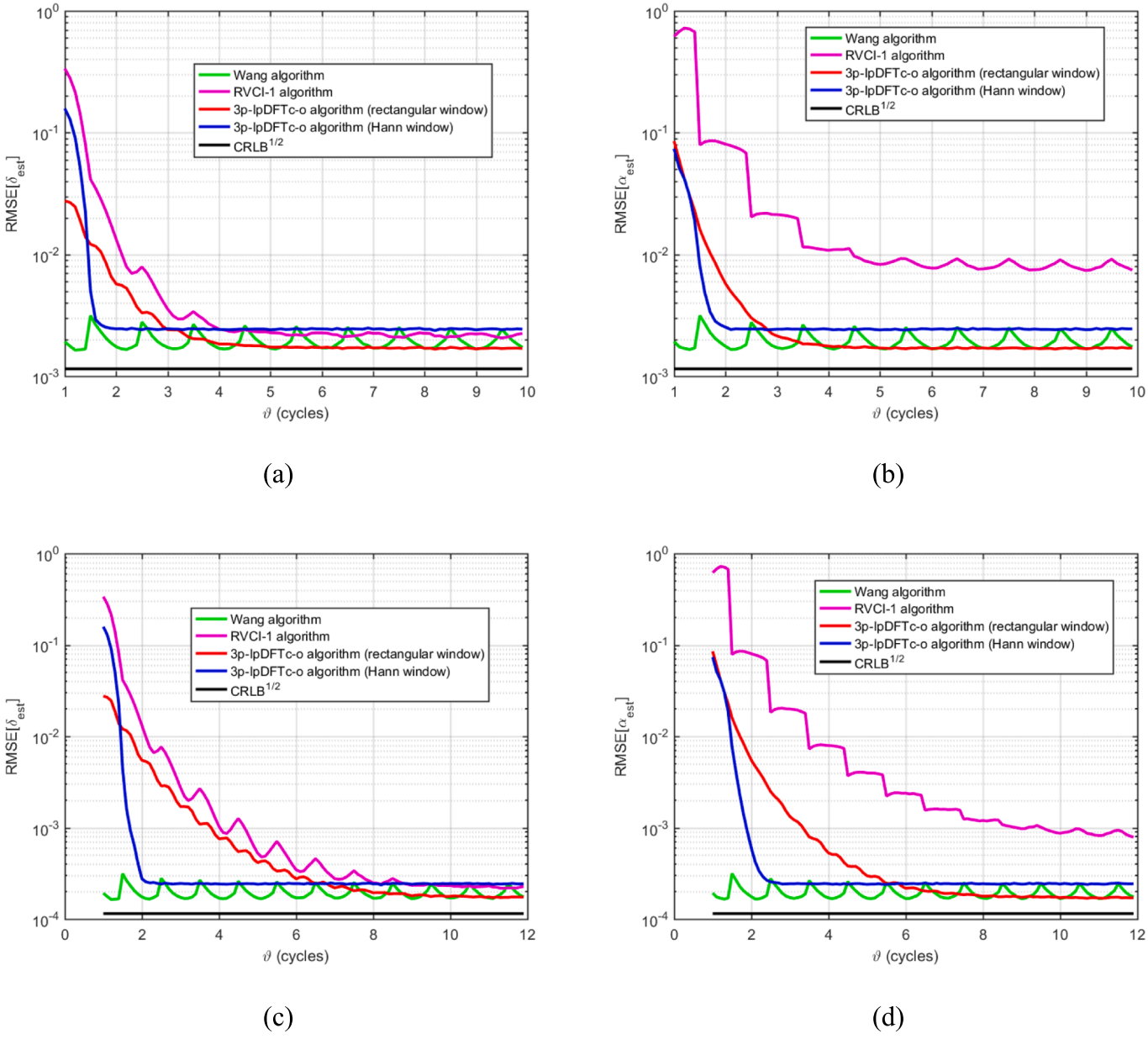

Fig. 9. Noisy damped sinusoids: simulation results for the *RMSE*s of the inter-bin frequency and the damping factor estimators versus the number of analyzed cycles when $SNR = 40$ dB (a), (b) and $SNR = 60$ dB (c), (d). Wang algorithm [16], RVCI-1 algorithm [3], 3p-IpDTFTc-o algorithm based on the rectangular and Hann windows. The asymptotic $\sqrt{CRLB}$ is also shown. Sinusoid amplitude $A = 1$ p.u. and damping factor $\alpha = 0.5$. 10,000 runs of $M = 512$ samples each with signal phase chosen at random.

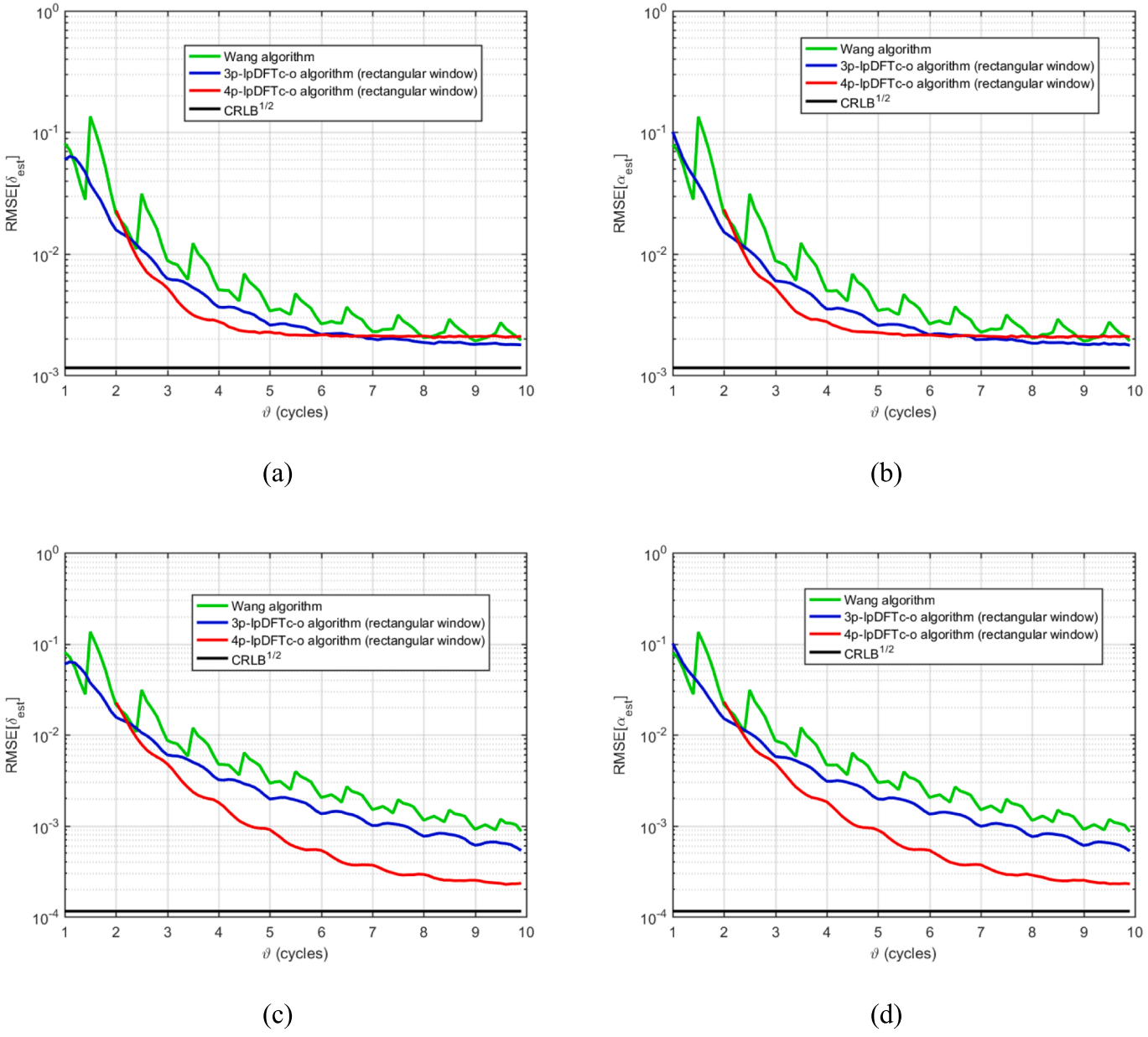

Fig. 10. Noisy and harmonically distorted damped sinusoids: simulation results for the *RMSEs* of the inter-bin frequency and the damping factor estimators versus the number of analyzed cycles when $SNR = 40$ dB (a), (b) and $SNR = 60$ dB (c), (d). Wang algorithm [16] and proposed 3p-IpDTFTc-o and 4p-IpDTFTc-o algorithms based on the rectangular window. The asymptotic $\sqrt{CRLB}$ is also shown. Sinusoid amplitude $A = 1$ p.u. and damping factor $\alpha = 0.5$. 2nd and 3rd harmonics with amplitudes 10 % and 5 % of fundamental and damping factors 0.375 and 0.25. 10,000 runs of $M = 512$ samples each with signal phase chosen at random.

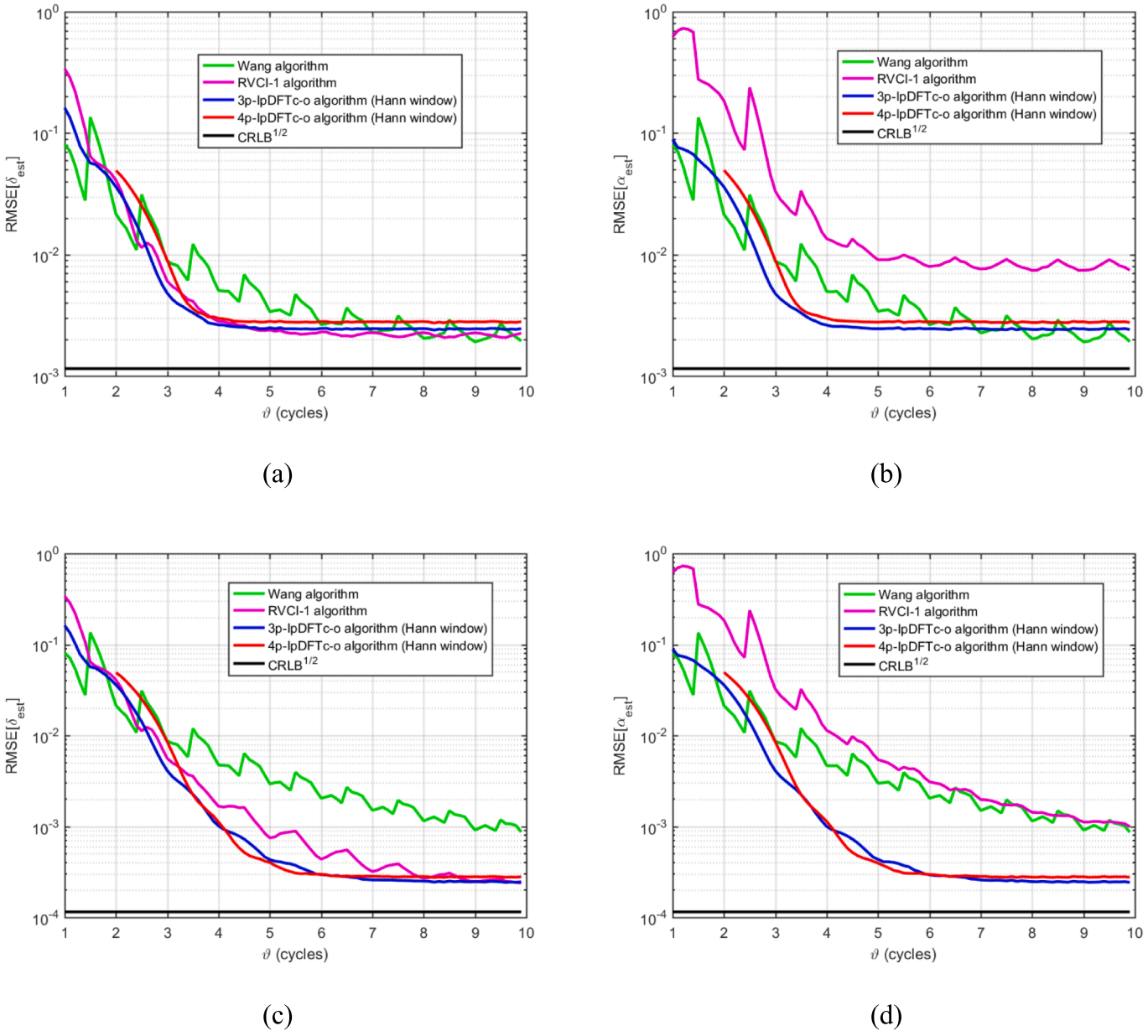

Fig. 11. Noisy and harmonically distorted damped sinusoids: simulation results for the *RMSEs* of the inter-bin frequency and the damping factor estimators versus the number of analyzed cycles when $SNR = 40$ dB (a), (b) and $SNR = 60$ dB (c), (d). Wang algorithm [16], RVCI-1 algorithm [3], and proposed 3p-IpDTFTc-o and 4p-IpDTFTc-o algorithms based on the Hann window. The asymptotic $\sqrt{CRLB}$ is also shown. Sinusoid amplitude $A = 1$ p.u. and damping factor $\alpha = 0.5$. 2nd and 3rd harmonics with amplitudes 10 % and 5 % of fundamental and damping factors 0.375 and 0.25. 10,000 runs of $M = 512$ samples each with signal phase chosen at random.

Table 1
Overall computational complexity required by the considered algorithms expressed in terms of number of RVAs and RVMs. Rectangular window.

Frequency estimator	RVAs	RVMs
Wang	$3M\log_2 M + M$	$2M\log_2 M + 2M$
3p- IpDTFTc-o	$3M\log_2 M + 7M - 6$	$2M\log_2 M + 8M$
4p- IpDTFTc-o	$3M\log_2 M + 9M - 8$	$2M\log_2 M + 10M$

algorithm may return more accurate estimates only for very short observation intervals, a situation where the contribution of the interference from the fundamental image component largely dominates the effect of wideband noise. Conversely, if the damped sinusoid is distorted by significant harmonics, the IpDTFTc-o algorithms based on either the rectangular window, or the Hann window outperforms the Wang algorithm in almost all considered simulation conditions. Thanks to their simple implementation and the low processing effort required, the proposed multi-point IpDTFTc-o algorithms can be employed in real-time low-cost hardware platforms for frequency and damping factor estimation of damped sinusoids.

CRediT authorship contribution statement

Daniel Belega: Writing – original draft, Validation, Software, Methodology, Investigation, Formal analysis, Conceptualization. **Dario Petri:** Writing – review & editing, Validation, Supervision, Methodology, Formal analysis. **Dominique Dallet:** Validation, Supervision, Methodology.

Declaration of competing interest

The authors declare that they have no known competing financial interests or personal relationships that could have appeared to influence the work reported in this paper.

Data availability

No data was used for the research described in the article.

Appendix A

Proof of the Theorem

Assuming (as often occurs in practice) that the *SNR* is enough high so that the contribution of wideband noise can be neglected, the interpolation multi-point function (8) becomes:

$$\widehat{\delta}-r+\mathrm{j}\widehat{\alpha}\cong\frac{\sum_{p=-K_1}^{K_1}a_pX_w(l+r+p)}{\sum_{q=-K_2}^{K_2}b_qX_w(l+r+q)}. \tag{A.1}$$

Using (6), (A.1) can be written as:

$$\widehat{\delta}-r+\mathrm{j}\widehat{\alpha}\cong\frac{\sum_{p=-K_1}^{K_1}a_p\psi(\alpha-\mathrm{j}(\delta-r)+\mathrm{j}p)\mathrm{e}^{\mathrm{j}\phi}+\sum_{p=-K_1}^{K_1}a_p\psi(\alpha+\mathrm{j}(2l+\delta+r)+\mathrm{j}p)\mathrm{e}^{-\mathrm{j}\phi}}{\sum_{q=-K_2}^{K_2}b_q\psi(\alpha-\mathrm{j}(\delta-r)+\mathrm{j}q)\mathrm{e}^{\mathrm{j}\phi}+\sum_{q=-K_2}^{K_2}b_q\psi(\alpha+\mathrm{j}(2l+\delta+r)+\mathrm{j}q)\mathrm{e}^{-\mathrm{j}\phi}}=\frac{f(\alpha-\mathrm{j}(\delta-r))\mathrm{e}^{\mathrm{j}\phi}+f(\alpha+\mathrm{j}(2l+\delta+r))\mathrm{e}^{-\mathrm{j}\phi}}{g(\alpha-\mathrm{j}(\delta-r))\mathrm{e}^{\mathrm{j}\phi}+g(\alpha+\mathrm{j}(2l+\delta+r))\mathrm{e}^{-\mathrm{j}\phi}}, \tag{A.2}$$

where $f(\nu)\overset{\mathrm{def}}{=}\sum_{p=-K_1}^{K_1}a_p\psi(\nu+\mathrm{j}p)$, and $g(\nu)\overset{\mathrm{def}}{=}\sum_{q=-K_2}^{K_2}b_q\psi(\nu+\mathrm{j}q)$.

From (A.2) it follows:

$$\widehat{\delta}-r+\mathrm{j}\widehat{\alpha}\cong\frac{f(\alpha-\mathrm{j}(\delta-r))}{g(\alpha-\mathrm{j}(\delta-r))}\frac{1+\frac{f(\alpha+\mathrm{j}(2l+\delta+r))}{f(\alpha-\mathrm{j}(\delta-r))}\mathrm{e}^{-\mathrm{j}2\phi}}{1+\frac{g(\alpha+\mathrm{j}(2l+\delta+r))}{g(\alpha-\mathrm{j}(\delta-r))}\mathrm{e}^{-\mathrm{j}2\phi}}. \tag{A.3}$$

Since $\left|\frac{g(\alpha+\mathrm{j}(2l+\delta+r))}{g(\alpha-\mathrm{j}(\delta-r))}\right|\ll1$, when l is not too small, using the approximation $(1+x)^{-1}\cong1-x$, which holds when $|x|\ll1$, and observing that the cross-product term can be neglected since it is much smaller than the others, it results:

$$\widehat{\delta}-r+\mathrm{j}\widehat{\alpha}\cong\frac{f(\alpha-\mathrm{j}(\delta-r))}{g(\alpha-\mathrm{j}(\delta-r))}\left[1+\frac{f(\alpha+\mathrm{j}(2l+\delta+r))}{f(\alpha-\mathrm{j}(\delta-r))}\mathrm{e}^{-\mathrm{j}2\phi}-\frac{g(\alpha+\mathrm{j}(2l+\delta+r))}{g(\alpha-\mathrm{j}(\delta-r))}\mathrm{e}^{-\mathrm{j}2\phi}\right]. \tag{A.4}$$

Let's consider now the expression of $\psi(\bullet)$given by (7). Since, in the considered conditions, the contribution of the image frequency component on $f(\alpha-\mathrm{j}(\delta-r))$ and $g(\alpha-\mathrm{j}(\delta-r))$ can be neglected, we have $\frac{f(\alpha-\mathrm{j}(\delta-r))}{g(\alpha-\mathrm{j}(\delta-r))}=\delta-r+\mathrm{j}$. Similarly, if the contribution of the fundamental component on $f(\alpha+\mathrm{j}(2l+\delta+r))$ and $g(\alpha+\mathrm{j}(2l+\delta+r))$ is negligible we have $\frac{f(\alpha+\mathrm{j}(2l+\delta+r))}{g(\alpha+\mathrm{j}(2l+\delta+r))}=-(\delta+2l+r)+\mathrm{j}\alpha$. By dividing the equalities above we obtain:

$$\frac{g(\alpha+\mathrm{j}(2l+\delta+r))}{g(\alpha-\mathrm{j}(\delta-r))}=\frac{\delta-r+\mathrm{j}\alpha}{-(\delta+2l+r)+\mathrm{j}\alpha}\frac{f(\alpha+\mathrm{j}(2l+\delta+r))}{f(\alpha-\mathrm{j}(\delta-r))} \tag{A.5}$$

By replacing $\frac{f(\alpha-\mathrm{j}(\delta-r))}{g(\alpha-\mathrm{j}(\delta-r))}=\delta-r+\mathrm{j}\alpha$ and the ratio (A.5) into (A.4) after simple algebra it follows:

$$\widehat{\delta}-r+\mathrm{j}\widehat{\alpha}\cong\delta-r+\mathrm{j}\alpha-2(l+\delta)\frac{\delta-r+\mathrm{j}\alpha}{-(\delta+2l+r)+\mathrm{j}\alpha}\frac{f(\alpha+\mathrm{j}(2l+\delta+r))}{f(\alpha-\mathrm{j}(\delta-r))}\mathrm{e}^{-\mathrm{j}2\phi} \tag{A.6.a}$$

or

$$\widehat{\delta}-r+\mathrm{j}\widehat{\alpha}\cong\delta-r+\mathrm{j}\alpha-2(l+\delta)\frac{g(\alpha+\mathrm{j}(2l+\delta+r))}{g(\alpha-\mathrm{j}(\delta-r))}\mathrm{e}^{-\mathrm{j}2\phi} \tag{A.6.b}$$

From (A.6.a) and (A.6.b), (9.a) and (9.b) can be easily derived.

Appendix B

Proof of the Proposition

If the number of observed signal cycles and the *SNR* are not too small, the contributions of the fundamental image component and noise to DFT samples employed in (13) can be neglected. Thus, (13) can be written as:

$$h\cong\frac{-(H+1)\widetilde{X}_w(l-2)+(H+2)\widetilde{X}_w(l-1)+(H-1)\widetilde{X}_w(l)-H\widetilde{X}_w(l+1)}{\widetilde{X}_w(l-2)-3\widetilde{X}_w(l-1)+3\widetilde{X}_w(l)-\widetilde{X}_w(l+1)}. \tag{B.1}$$

By using (6), after some algebra the following equalities are achieved:

$$\widetilde{X}_w(l-2)=\frac{(\alpha-\mathrm{j}\delta+\mathrm{j}(H-1))(\alpha-\mathrm{j}\delta+j(H-2))}{(\alpha-\mathrm{j}\delta-\mathrm{j}H)(\alpha-\mathrm{j}\delta-\mathrm{j}(H+1))}\widetilde{X}_w(l), \tag{B.2.a}$$

$$\widetilde{X}_w(l-1)=\frac{\alpha-\mathrm{j}\delta+\mathrm{j}(H-1)}{\alpha-\mathrm{j}\delta-\mathrm{j}H}\widetilde{X}_w(l), \tag{B.2.b}$$

$$\widetilde{X}_w(l+1) = \frac{\alpha - \mathrm{j}\delta - \mathrm{j}(H-1)}{\alpha - \mathrm{j}\delta + \mathrm{j}H}\widetilde{X}_w(l). \tag{B.2.c}$$

By using the above equalities, after tedious calculation we obtain:

$$-(H+1)\widetilde{X}_w(l-2)+(H+2)\widetilde{X}_w(l-1)+(H-1)\widetilde{X}_w(l)-H\widetilde{X}_w(l+1) = \frac{2H\left(4H^2-1\right)(\alpha-\mathrm{j}\delta)}{(\alpha-\mathrm{j}\delta-\mathrm{j}H)(\alpha-\mathrm{j}\delta+\mathrm{j}H)(\alpha-\mathrm{j}\delta-\mathrm{j}(H+1))}, \tag{B.3.a}$$

$$\widetilde{X}_w(l-2) - 3\widetilde{X}_w(l-1) + 3\widetilde{X}_w(l) - \widetilde{X}_w(l+1) = -\frac{2H\left(4H^2-1\right)\mathrm{j}}{(\alpha-\mathrm{j}\delta-\mathrm{j}H)(\alpha-\mathrm{j}\delta+\mathrm{j}H)(\alpha-\mathrm{j}\delta-\mathrm{j}(H+1))}. \tag{B.3.b}$$

By replacing (B.3.a) and (B.3.b) into (B.1) we have:

$$h \cong \delta + \mathrm{j}\alpha. \tag{B.4}$$

Thus, (B.4) shows that (13) is the interpolation function of a 4p-IpDFT algorithm based on the H-term MSD window.

References

[1] H. Günther, NMR Spectroscopy: Basic Principles, Concepts and Applications in Chemistry, John Wiley & Sons, 2013.
[2] J.C. Visschers, E. Wilson, T. Connelly, A. Mudrov, L. Bougasi, Rapid parameter determination of discrete damped sinusoidal oscillations, Opt. Express 29 (5) (2021) 6863–6878.
[3] K. Duda, T.P. Zielinski, L.B. Magalas, M. Majewski, DFT based estimation of damped oscillation's parameters in low frequency mechanical spectroscopy, IEEE Trans. Instrum. Meas. 60 (11) (2011) 3608–3618.
[4] K. Duda, T.P. Zielinski, Efficacy of the frequency and damping estimation of a real-value sinusoid, IEEE Instrum. Meas. Mag. 16 (2) (2013) 48–58.
[5] E. Aboutanios, Estimation of the frequency and decay factor of a decaying exponential in noise, IEEE Trans. Signal Process. 58 (2) (2010) 501–509.
[6] Y. Hua, T.K. Sarkar, Matrix pencil method for estimating parameters of exponentially damped/undamped sinusoid in noise, IEEE Trans. Acoust. Speech Signal Process. 38 (5) (1990) 814–824.
[7] P. Chen, X. Su, T. Shen, L. Mou, A parameter estimation algorithm for damped real-valued sinusoid in noise, Measur. Sci. Rev. 23 (3) (2023) 99–105.
[8] M. Bertocco, C. Offeli, D. Petri, Analysis of damped sinusoidal signals via a frequency-domain interpolation algorithm, IEEE Trans. Instrum. Meas. 43 (2) (1994) 245–250.
[9] R. Diao, Q. Meng, An interpolation algorithm for discrete Fourier transforms of weighted damped sinusoidal signals, IEEE Trans. Instrum. Meas. 63 (6) (2014) 1505–1523.
[10] R. Diao, Q. Meng, H. Fan, Interpolation algorithms based on Rife-Vincent window for discrete Fourier transforms of damped signals (in Chinese), J. Mech. Eng. 51 (4) (2015).
[11] D. Agrež, Estimation of parameters of the weakly damped sinusoidal signals in the frequency domain, Comput. Stand. Interfaces 33 (2011) 117–121.
[12] I. Yoshida, T. Sugai, S. Tani, M. Motegi, K. Minamida, H. Hayakawa, Automation of internal friction measurement apparatus of inverted torsion pendulum type, J. Phys. E Sci. Instrum. 14 (10) (1981) 1201–1206.
[13] K. Wang, H. Wen, L. Xu, L. Wang, Two points interpolated DFT algorithm for accurate estimation of damping factor and frequency, IEEE Signal Process. Lett. 28 (2021) 499–502.
[14] J. Song, A. Mingotti, J. Zhang, L. Peretto, H. Wen, Accurate damping factor and frequency estimation for damped real-valued sinusoidal signals, IEEE Trans. Instrum. Meas. 71 (2022).
[15] D. Belega, D. Petri, Fast interpolated DTFT estimators of frequency and damping factor of real-valued damped sinusoids, Measurement 217 (2023).
[16] K. Wang, H. Wen, W. Tai, G. Li, Estimation of damping factor and signal frequency for damped sinusoidal signal by three points interpolated DFT, IEEE Signal Process. Lett. 29 (12) (2019) 1927–1930.
[17] H. Xu, S. Zhou, B. Yan, Parameter estimation for a damped real-valued sinusoid in noise, Rev. Sci. Instrum. 92 (2021).
[18] D. Belega, D. Petri, D. Dallet, Accurate frequency and damping factor estimation by means of an improved three-point interpolated DFT algorithm, in: Proc. IMEKO TC4 conference, Pordenone, 20–21 Sept. 2023.
[19] A.H. Nuttall, Some windows with very good sidelobe behavior, IEEE Trans. Acoust. Speech Signal Process. ASSP 29 (1) (1981) 84–91.
[20] F.J. Harris, On the use of windows for harmonic analysis with the discrete Fourier transform, Proc. IEEE 66 (1) (1978) 51–83.
[21] D. Agrež, Dynamics of frequency estimation in the frequency domain, IEEE Trans. Instrum. Meas. 51 (2) (2007) 287–292.
[22] E. Jacobsen, P. Kootsookos, Fast, accurate frequency estimators, IEEE Signal Process. Mag. 24 (2007) 123–125.
[23] C. Candan, A method for fine resolution frequency estimation from three DFT samples, IEEE Signal Process. Lett. 18 (6) (2011) 351–354.
[24] D. Belega, D. Petri, Frequency estimation by two- or three-point interpolated Fourier algorithms based on cosine windows, Signal Process. 114 (2015) 115–125.
[25] D. Belega, D. Dallet, Multifrequency signal analysis by interpolated DFT method with maximum sidelobe decay windows, Measurement 42 (3) (2009) 420–426.
[26] Y. Yao, S.M. Pandit, Cramér-Rao lower bounds for a damped sinusoidal process, IEEE Trans. Signal Process. 43 (4) (1995) 878–885.
[27] D. Belega, D. Petri, Effect of noise and harmonics on sine-wave frequency estimation by interpolated DFT algorithms based on few observed cycles, Signal Proces. 140 (2017) 207–218.
[28] D. Manolakis, V. Ingle, Applied Digital Signal Processing, Cambridge University Press, 2011.